



Cite this: DOI: 10.1039/c8nj01333k

Synthesis of *N*-[(2-hydroxyethoxy)carbonyl]glycine from carbon dioxide, ethylene oxide, and α -amino acid by ionic gelation of sodium tripolyphosphate (TPP) and spirulina supported on magnetic KCC-1 in aqueous solution

Rahele Zhiani,^a Mehdi Khoobi^{b,c} and Seyed Mohsen Sadeghzadeh  ^{*a}

In this study, a novel ionic gelation (IG) of sodium tripolyphosphate (TPP) and spirulina was prepared that, supported on magnetic fibrous silica nanospheres (Fe₃O₄/KCC-1/IG), has been developed for the synthesis of *N*-[(2-hydroxyethoxy)carbonyl]glycine from carbon dioxide, ethylene oxide, and α -amino acid. This morphology ultimately leads to higher catalytic activity for the KCC-1-supported ionic gelation. The Fe₃O₄/KCC-1/IG MNPs were thoroughly characterized by using TEM, FESEM, VSM, FT-IR, TGA, and BET. We supported an ionic gelation on the surface of silica and used spirulina and TPP as a catalyst; the observations were exploited in the direct and selective chemical fixation of CO₂ to afford high degrees of CO₂ capture and conversion.

Received 18th March 2018,
Accepted 9th May 2018

DOI: 10.1039/c8nj01333k

rsc.li/njc

Introduction

The conversion of carbon dioxide into value-added organic compounds continues to be a vivid area of research in academic and industrial settings. The valorization of CO₂ is important to create value from a waste material, and current efforts have already shown great potential towards the use of CO₂ to store energy, and as a synthon for the creation of new polymers and fine chemicals. Another area of widespread interest and importance concerns the preparation of organic carbonates. More recently, focus has been shifted towards the use of these carbonates as intermediates in organic synthesis.^{1–19} An attractive route towards the conversion of cyclic carbonates into useful products concerns their aminolysis by aliphatic amines, thus affording *N*-alkyl carbamate structures.^{20–24}

Algae are naturally abundant and found in all kinds of aquatic environments. Among algae species, *Spirulina platensis* is a photosynthetic, filamentous, spiral-shaped, multicellular, and bluegreen microalgae. Spirulina filaments may be easily separated from their medium, have high digestibility and a mild flavor, and contain up to 70% excellent quality protein.

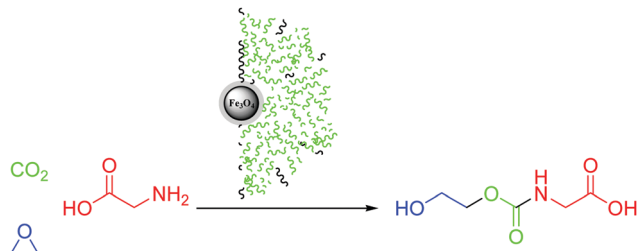
They contain reactive (amino and hydroxyl) functional groups, providing biocompatibility, low-toxicity and pH-sensitivity, as well as metal anchoring functional groups.^{25–28}

The incorporation of magnetic nanoparticles (MNPs) into an amino and hydroxyl group containing network, using a poly-anionic cross-linker such as tripolyphosphate (TPP),^{29–31} allows the interaction of MNPs with the cationic spirulina through electrostatic interactions; at the same time, spirulina forms strong interactions with MNPs because of its good chelating ability with metal ions. The use of a physical cross-linking agent (TPP) instead of a chemical cross-linker (such as glutaraldehyde) prevents toxicity of the reagents. Recently, Polshettiwar *et al.*³² reported a novel fibrous silica nanosphere (KCC-1) material, which has special center-radial pore structures with the pore sizes gradually increasing from the center to the surface. The KCC-1 material showed high specific surface area due to the pores in the fibers, and the accessibility of the active sites was significantly increased as a result of the special structure.^{33–37} Additionally, the 3-D architecture-generated hierarchical pore structure with macropores can also improve the mass transfer of the reactant.^{38,39} The KCC-1-based sorbents may have several advantages over conventional silica-based sorbents, including (i) high catalyst loading, (ii) minimum reduction in surface area after functionalization and (iii) more accessibility of the catalyst sites to enhance the reaction, due to the fibrous structure and highly accessible surface area of KCC-1. Given our continued interest in nanocatalysis and catalyst development for organic reactions,^{40–48} we reported the preparation and characterization

^a Young Researchers and Elite Club, Neyshabur Branch, Islamic Azad University, Neyshabur, Iran. E-mail: seyedmohsen.sadeghzadeh@gmail.com

^b The Institute of Pharmaceutical Sciences (TIPS), Tehran University of Medical Sciences, Tehran 1417614411, Iran

^c Department of Pharmaceutical Biomaterials, Faculty of Pharmacy, Tehran University of Medical Sciences, Tehran, Iran



Scheme 1 Synthesis of *N*-[(2-hydroxyethoxy)carbonyl]glycine in the presence of $\text{Fe}_3\text{O}_4/\text{KCC-1/IG}$ MNPs.

of novel ionic gelation (IG) of sodium tripolyphosphate (TPP) and spirulina supported on $\text{Fe}_3\text{O}_4/\text{KCC-1}$ magnetic nanoparticles. In addition, we described its utility for *N*-[(2-hydroxyethoxy)carbonyl]glycine synthesis from CO_2 , ethylene oxide, and α -amino acids, and it could be easily separated from the reaction mixture for reuse (Scheme 1).

Experimental

Materials and methods

Chemical materials were purchased from Fluka and Merck in high purity. Melting points were determined in open capillaries using an Electrothermal 9100 apparatus and are uncorrected. FTIR spectra were recorded on a VERTEX 70 spectrometer (Bruker) in the transmission mode in spectroscopic grade KBr pellets for all the powders. The nitrogen adsorption/desorption isotherms were measured at liquid nitrogen temperature (-196°C) using a PHS-1020 (PHSCHINA) instrument. The particle size and structure of the nano particles was observed by a TESCAN MIRA field emission scanning electron microscope (FE-SEM) with a gold coating and high-resolution transmission electron microscopy (HRTEM) was performed on a Philips CN120 device. Powder X-ray diffraction data were obtained using a Bruker D8 Advance model with $\text{Cu K}\alpha$ radiation. Thermogravimetric analysis (TGA) was carried out on a NETZSCH STA449F3 at a heating rate of $10^\circ\text{C min}^{-1}$ under nitrogen. ^1H and ^{13}C NMR spectra were recorded on a BRUKER DRX-300 AVANCE spectrometer at 300.13 and 75.46 MHz, and a BRUKER DRX-400 AVANCE spectrometer at 400.22 and 100.63 MHz, respectively. Elemental analyses for C, H, and N were performed using a Heraeus CHN-O-rapid analyzer. The purity determination of the products and reaction monitoring were accomplished by TLC on silica gel polygram SILG/UV 254 plates. Mass spectra were recorded on a Shimadzu GCMS-QP5050 Mass Spectrometer.

General procedure for the preparation of Fe_3O_4 MNPs

The synthesis procedure is illustrated as follows: (1) 0.01 mol $\text{FeCl}_2\cdot 4\text{H}_2\text{O}$ and 0.03 mol $\text{FeCl}_3\cdot 6\text{H}_2\text{O}$ were dissolved in 200 mL distilled water, followed by the addition of polyethylene glycol (PEG) (1.0 g, M_w 6000). (2) Sodium hydroxide (NaOH) was added to this solution and the pH value was controlled in the range $12 \leq \text{pH} \leq 13$. (3) Different amounts of hydrazine hydrate ($\text{N}_2\text{H}_4\cdot\text{H}_2\text{O}$, 80% concentration) were added to the

above suspension. The reaction was continued for about 24 h at room temperature. During this period, the pH value was adjusted by NaOH and kept in the range $12 \leq \text{pH} \leq 13$. The black Fe_3O_4 NPs were then rinsed several times with ionized water.

General procedure for the preparation of $\text{Fe}_3\text{O}_4/\text{SiO}_2$ MNPs

0.02 mol of Fe_3O_4 MNPs were dispersed in a mixture of 80 mL of ethanol, 20 mL of deionized water and 2.0 mL of 28 wt% concentrated ammonia aqueous solution ($\text{NH}_3\cdot\text{H}_2\text{O}$), followed by the addition of 0.20 g of tetraethyl orthosilicate (TEOS). After vigorous stirring for 24 h, the final suspension was repeatedly washed, filtered several times and dried at 60°C in air.

General procedure for the preparation of $\text{Fe}_3\text{O}_4/\text{SiO}_2/\text{KCC-1}$ MNPs

$\text{Fe}_3\text{O}_4/\text{SiO}_2$ (0.25 g) was dispersed in an aqueous solution (30 mL) containing urea (0.3 g) to form solution A under ultrasonication for 1 h. Cetylpyridinium bromide (CPB) (0.5 g) was added to 0.75 mL of *n*-pentanol and 30 mL cyclohexane to form solution B. Solution A was added to solution B under stirring at room temperature. Then 1.25 g TEOS was added drop wise to the abovementioned solution. The resulting mixture was continually stirred for 1 h at room temperature and then placed in a 120°C environment for 5 h, thus initiating the reaction. After the reaction was completed, the mixture was allowed to cool to room temperature, and the $\text{Fe}_3\text{O}_4/\text{SiO}_2/\text{KCC-1}$ core-shell microspheres were isolated by strong magnetic suction, then washed with deionized water and acetone, and dried overnight in a drying oven at 40°C . This material was then calcined at 550°C for 5 h in air.

General procedure for the preparation of $\text{Fe}_3\text{O}_4/\text{KCC-1/IG}$ MNPs

$\text{Fe}_3\text{O}_4/\text{KCC-1}$ (50 mg) was dispersed in acetic acid solution by ultrasonication for 1 min. Spirulina (125 mg) was dissolved in the same acetic acid solution and stirred at room temperature for 1 h. TPP solution (10 mL) was injected dropwise into the chitosan solution using a syringe pump with a 1 mL min^{-1} rate of injection. After complete addition of TPP, the mixture was kept stirring mechanically (1000 rpm) for 1 h. The formed product was collected with an external magnet and washed with water until pH 7 and dried under vacuum at room temperature for 24 h.

General procedure for synthesis of *N*-[(2-hydroxyethoxy)carbonyl]glycine

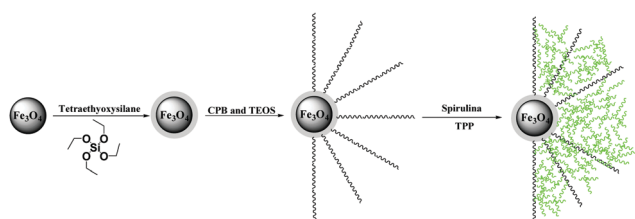
1.0 MPa of CO_2 , 1.0 mmol of α -amino acid, 1.0 mmol of ethylene oxide, and 10 mg of $\text{Fe}_3\text{O}_4/\text{KCC-1/IG}$ MNPs were properly added at room temperature. Then, to keep a constant pressure of 2.0 MPa, CO_2 was added from a reservoir tank and the temperature was increased to 100°C . The remaining CO_2 was slowly removed and the catalyst was segregated through filtration under vacuum after the reaction to be further used for the recycling experiments. After drying the resultant crude product over anhydrous sodium sulphate, the mixture was subjected to column chromatography (CC) using a system of petroleum ether/EtOAc as an eluent (6:1) on silica gel.

Results and discussion

The $\text{Fe}_3\text{O}_4/\text{KCC-1}$ core-shell was synthesized by a simple method and then functionalized by the ionic gelation (IG) of sodium tripolyphosphate (TPP) and spirulina, according to Scheme 2. The synthesized $\text{Fe}_3\text{O}_4/\text{KCC-1}/\text{IG}$ MNPs were then characterized by different methods such as TEM, FESEM, VSM, FT-IR, TGA, and BET (Scheme 2).

The morphology and structure of the $\text{Fe}_3\text{O}_4/\text{KCC-1}$, $\text{Fe}_3\text{O}_4/\text{SiO}_2/\text{IG}$, and $\text{Fe}_3\text{O}_4/\text{KCC-1}/\text{IG}$ MNPs are further characterized by TEM and FE-SEM. As shown in Fig. 1f, the $\text{Fe}_3\text{O}_4/\text{KCC-1}$ possesses a core of Fe_3O_4 particles, a nonporous silica layer and silica fibres. The as-prepared magnetic core-shell fibrous silica material $\text{Fe}_3\text{O}_4/\text{KCC-1}$ with a fibrous structure was uniform and monodispersed. Also, TEM and FE-SEM images of the highly textured $\text{Fe}_3\text{O}_4/\text{KCC-1}$ samples show that the samples have spheres of uniform size with diameters of ~ 300 nm and a wrinkled radial structure (Fig. 1a and f). A close inspection of these images shows that wrinkled fibers (with thicknesses of ~ 8.5 nm) grow out from the center of the spheres and are arranged radially in three dimensions. Also, the overlapping of the wrinkled radial structures forms cone-shaped open pores. The TEM and FE-SEM images show that the entire sphere is solid and composed of fibers. Furthermore, these open hierarchical channel structures and fibers make the mass transfer of reactants easier and increase the accessibility of active sites. The FE-SEM and TEM images of $\text{Fe}_3\text{O}_4/\text{KCC-1}/\text{IG}$ MNPs showed that after modification the morphology of $\text{Fe}_3\text{O}_4/\text{KCC-1}$ is not changed (Fig. 1b and g). To assess the exact impact of the presence of KCC-1 in the catalyst, the $\text{Fe}_3\text{O}_4/\text{KCC-1}/\text{IG}$ was compared with $\text{Fe}_3\text{O}_4/\text{SiO}_2/\text{IG}$ MNPs. To further understand this issue, FE-SEM and TEM images of the used catalyst were compared with those of the fresh catalyst. This comparison of the FE-SEM and TEM images of the used catalyst with those of the fresh catalyst showed that the morphologies and structures of $\text{Fe}_3\text{O}_4/\text{KCC-1}/\text{IG}$ (Fig. 1d and i) and $\text{Fe}_3\text{O}_4/\text{SiO}_2/\text{IG}$ MNPs remained intact after ten recoveries (Fig. 1e and j). Fig. 1e and j show the degradation of the structure of the $\text{Fe}_3\text{O}_4/\text{SiO}_2/\text{IG}$ MNPs in the reuse process. Their structure has been destroyed. But, the functionalization of the $\text{Fe}_3\text{O}_4/\text{KCC-1}/\text{IG}$ MNPs does not result in the change of the morphology (Fig. 1c and h). This study proves that the stability of the structure of $\text{Fe}_3\text{O}_4/\text{KCC-1}/\text{IG}$ MNPs was due to the presence of KCC-1 in the catalyst structure. KCC-1 can be a strong scaffold in ionic gelation structures.

The powder X-ray diffraction patterns of Fe_3O_4 , $\text{Fe}_3\text{O}_4/\text{KCC-1}$, and $\text{Fe}_3\text{O}_4/\text{KCC-1}/\text{IG}$ MNPs are shown in Fig. 2. As can be observed,



Scheme 2 Schematic illustration of the synthesis for $\text{Fe}_3\text{O}_4/\text{KCC-1}/\text{IG}$ MNPs.

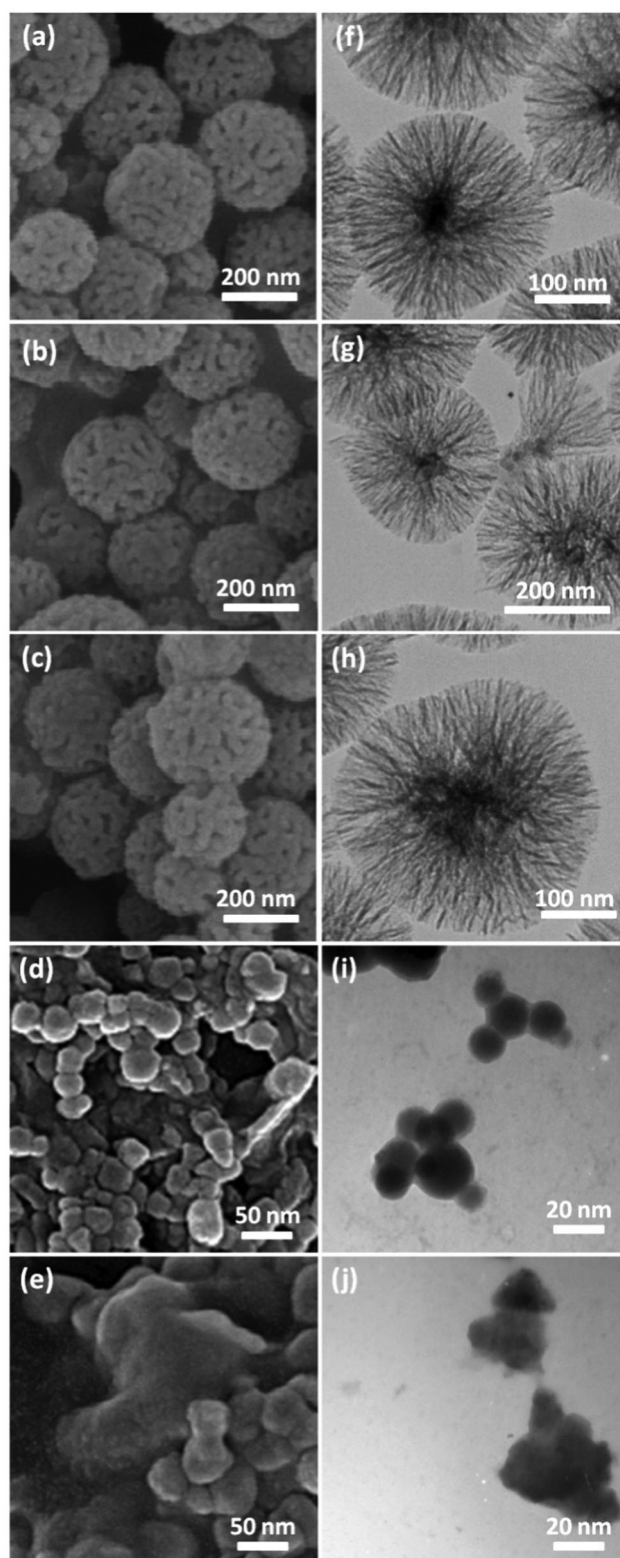


Fig. 1 FE-SEM images of $\text{Fe}_3\text{O}_4/\text{KCC-1}$ MNPs (a); fresh $\text{Fe}_3\text{O}_4/\text{KCC-1}/\text{IG}$ MNPs (b); $\text{Fe}_3\text{O}_4/\text{KCC-1}/\text{IG}$ MNPs after ten reuses (c); fresh $\text{Fe}_3\text{O}_4/\text{SiO}_2/\text{IG}$ MNPs (d); $\text{Fe}_3\text{O}_4/\text{SiO}_2/\text{IG}$ MNPs after ten reuses (e); TEM images of $\text{Fe}_3\text{O}_4/\text{KCC-1}$ MNPs (f); fresh $\text{Fe}_3\text{O}_4/\text{KCC-1}/\text{IG}$ MNPs (g); $\text{Fe}_3\text{O}_4/\text{KCC-1}/\text{IG}$ MNPs after ten reuses (h); fresh $\text{Fe}_3\text{O}_4/\text{SiO}_2/\text{IG}$ MNPs (i); $\text{Fe}_3\text{O}_4/\text{SiO}_2/\text{IG}$ MNPs after ten reuses (j).

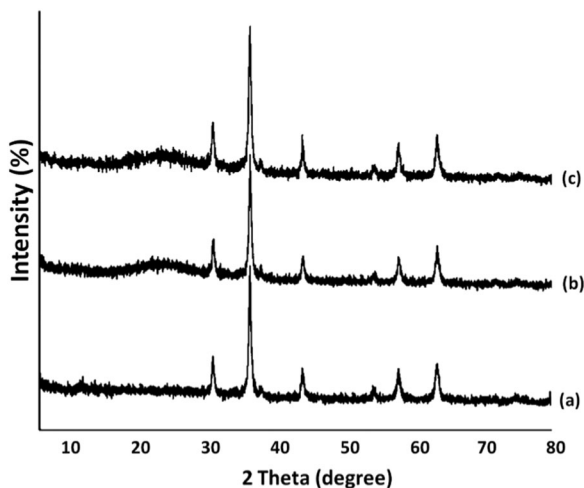


Fig. 2 XRD analysis of (a) Fe_3O_4 , (b) $\text{Fe}_3\text{O}_4/\text{KCC-1}$, and (c) $\text{Fe}_3\text{O}_4/\text{KCC-1}/\text{IG}$ MNPs.

all samples possess the typical diffraction peaks at (220), (311), (400), (422), (511) and (440), which are in good agreement with the data for a standard Fe_3O_4 sample, as reported in the JCPDS card (No. 19-0629) (Fig. 2a). Besides the peak of iron oxide, the XRD pattern of $\text{Fe}_3\text{O}_4/\text{KCC-1}$ core-shell nanoparticles presented a broad featureless XRD peak at low diffraction angle, which corresponded to amorphous silica (Fig. 2b). Fig. 2c shows a typical XRD pattern of the $\text{Fe}_3\text{O}_4/\text{KCC-1}/\text{IG}$ MNPs. There was no change in it.

The thermal behavior of $\text{Fe}_3\text{O}_4/\text{KCC-1}/\text{IG}$ MNPs is shown in Fig. 3. The weight loss below 150 °C was ascribed to the elimination of the physisorbed and chemisorbed solvent on the surface of both the $\text{Fe}_3\text{O}_4/\text{KCC-1}$ and $\text{Fe}_3\text{O}_4/\text{KCC-1}/\text{IG}$ MNPs materials. In the second stage (180–350 °C), the weight loss is about 13.4 wt%, which can be attributed to the organic group derivatives. TGA strongly supported the successful grafting of organoamine groups on the silica nanospheres as no weight loss was observed in the range of 150–500 °C for $\text{Fe}_3\text{O}_4/\text{KCC-1}$.

The magnetic properties of the nanoparticles were characterized using a vibrating sample magnetometer (VSM). The magnetization

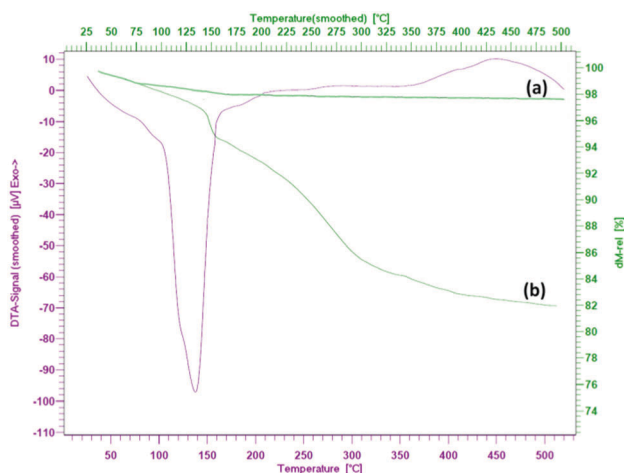


Fig. 3 TGA diagram of (a) $\text{Fe}_3\text{O}_4/\text{KCC-1}$, and (b) $\text{Fe}_3\text{O}_4/\text{KCC-1}/\text{IG}$ MNPs.

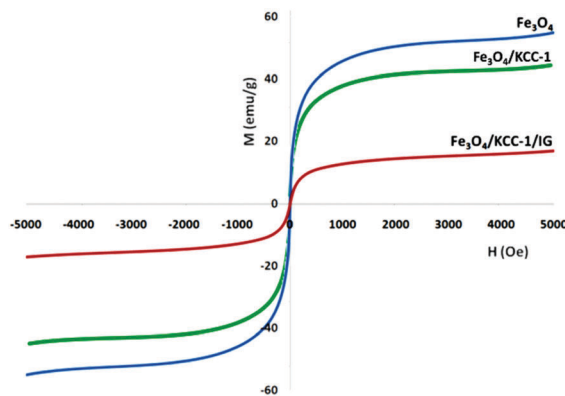


Fig. 4 Room-temperature magnetization curves of the nano catalysts.

curves of the obtained nanocomposite registered at 300 K show that nearly no residual magnetism is detected (Fig. 4), which means that the nanocomposite exhibited paramagnetic characteristics. Magnetic measurement shows that pure Fe_3O_4 , $\text{Fe}_3\text{O}_4/\text{KCC-1}$, and $\text{Fe}_3\text{O}_4/\text{KCC-1}/\text{IG}$ MNPs have saturation magnetization values of 55.3, 42.9 and 17.2 emu/g respectively. These nanocomposites with paramagnetic characteristics and high magnetization values can quickly respond to the external magnetic field and quickly redisperse once the external magnetic field is removed. The result reveals that the nanocomposites exhibit good magnetic response, which suggests a potential application for targeting and separation.

The N_2 adsorption–desorption isotherms of $\text{Fe}_3\text{O}_4/\text{KCC-1}/\text{IG}$ MNPs showed characteristic type IV curves (Fig. 5), which is consistent with the literature reports on standard fibrous silica spheres. As for $\text{Fe}_3\text{O}_4/\text{KCC-1}$, the BET surface area, total pore volume, and BJH pore diameter are obtained as 427 $\text{m}^2 \text{g}^{-1}$, 1.23 $\text{cm}^3 \text{g}^{-1}$ and 14.51 nm respectively, whereas the corresponding parameters of the $\text{Fe}_3\text{O}_4/\text{KCC-1}/\text{IG}$ MNPs have decreased to 172 $\text{m}^2 \text{g}^{-1}$, 0.85 $\text{cm}^3 \text{g}^{-1}$, and 10.03 nm. The nitrogen sorption analysis of $\text{Fe}_3\text{O}_4/\text{KCC-1}/\text{IG}$ MNPs also confirms a regular and uniform mesostructure with a decrease in surface area, pore diameter and pore volume parameters in comparison with that of pristine $\text{Fe}_3\text{O}_4/\text{KCC-1}$ MNPs. This could be ascribed to

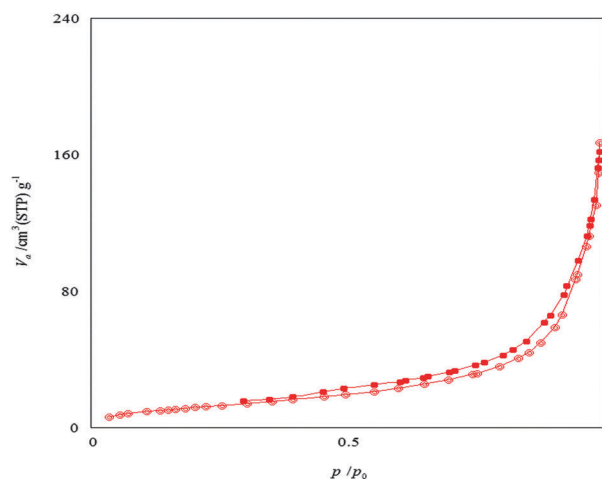


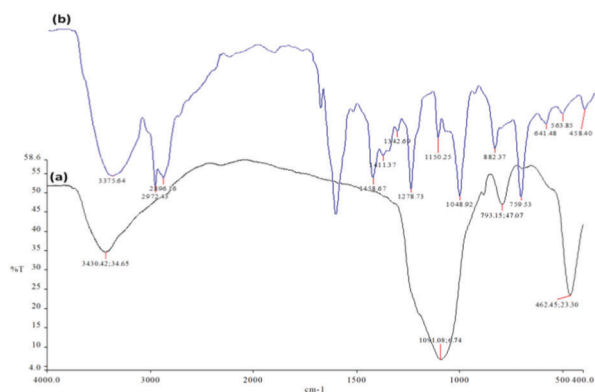
Fig. 5 Adsorption–desorption isotherms of $\text{Fe}_3\text{O}_4/\text{KCC-1}/\text{IG}$ MNPs.

Table 1 Structural parameters of Fe₃O₄/KCC-1 and Fe₃O₄/KCC-1/IG MNP materials determined from nitrogen sorption experiments

Catalysts	S_{BET} (m ² g ⁻¹)	V_a (cm ³ g ⁻¹)	D_{BJH} (nm)
Fe ₃ O ₄ /KCC-1	427	1.23	14.51
Fe ₃ O ₄ /KCC-1/IG	172	0.85	10.03
Fe ₃ O ₄ /KCC-1/IG after ten reuses	179	0.89	10.21

increased loading with the sensing probe, which occupies a large volume inside the silica spheres (Fig. 5 and Table 1). Comparison of the BET surface area, total pore volume, and BJH pore diameter of the used catalyst with those of the fresh catalyst showed that the structure of the catalyst remained intact after ten recoveries.

FT-IR spectroscopy was employed to determine the surface modification of the synthesized catalyst (Fig. 6). The symmetric and asymmetric stretching vibrations of Si–O–Si and the stretching vibration of O–H at 799, 1088, and 3394 cm⁻¹ were observed for Fe₃O₄/KCC-1, respectively (Fig. 6a). The FT-IR analyses of Fe₃O₄/KCC-1/IG represent the following functional groups. The FT-IR shows a frequency range from 3400–3300 cm⁻¹ representing the O–H stretching vibration. It shows the presence of carbohydrate and amino acid. The peaks in the frequency range of 3500–3300 cm⁻¹ represent the N–H stretching vibration, the presence of amines in proteins, and lipids. The bands observed at 2972 and 2896 cm⁻¹ are assigned to C–H stretching of aliphatic moieties. The peak that appeared at 1720 cm⁻¹ is due to the stretching of the C=O group in the ester and amino acid. The following peak at 1642 cm⁻¹ is attributed to the bending vibration of the N–H group present in the carbonyl β unsaturated ketone amide. The peak appearing at 1411 cm⁻¹ peak is the CH₂ bending vibration. The bands observed at 1342 cm⁻¹ and 1278 cm⁻¹ due to C–O stretching, O–H bending vibration, respectively, show the presence of alcohol. On functionalization with the tripolyphosphate, the intensity of the peak around 1048 cm⁻¹ increased and a new peak appeared at 882 cm⁻¹ which is relevant to phosphate and phosphoramidate groups, and it suggests reaction between $-\text{P}_3\text{O}_{10}^{5-}$ and $-\text{NH}_3^+$. The main differences in the IR spectra is the additional peak in the TPP bead spectrum at 1150 cm⁻¹, which can be assigned to the

**Fig. 6** FTIR spectra of (a) Fe₃O₄/KCC-1 MNPs, and (b) Fe₃O₄/KCC-1/IG MNPs.**Table 2** Influence of different catalysts for the synthesis of *N*-[(2-hydroxyethoxy)carbonyl]glycine^a

Entry	Catalyst	Yield ^b (%)
1	Fe ₃ O ₄ /KCC-1	—
2	Fe ₃ O ₄ /KCC-1/TPP	—
3	Fe ₃ O ₄ /KCC-1/spirulina	—
4	Fe ₃ O ₄ /KCC-1/IG	97
5	Fe ₃ O ₄ /SiO ₂ /IG	48

^a Reaction conditions: appropriate CO₂ (1.0 MPa), α -amino acid (1.0 mmol), ethylene oxide (1.0 mmol), Fe₃O₄/KCC-1/IG MNPs (10 mg), and CO₂ 1.0 MPa, at 100 °C. ^b Isolated yield.

–P=O stretching vibration indicating the presence of phosphate groups.

For further investigation on the efficiency of the catalyst in this reaction, different control experiments were performed and the obtained data are shown in Table 2. Initially, a standard reaction was carried out using Fe₃O₄/KCC-1 showing that no amount of the desired product was formed after 2 h of reaction time (Table 2, entry 1). Also, when Fe₃O₄/KCC-1/TPP was used as the catalyst, a reaction was not observed (Table 2, entry 2). The TPP could not give satisfactory catalytic activity under mild conditions. Based on these disappointing results, we continued the studies to improve the yield of the product by replacing the spirulina. The synthesis of *N*-[(2-hydroxyethoxy)carbonyl]glycine was not observed when the reaction was carried out using Fe₃O₄/KCC-1/TPP and Fe₃O₄/KCC-1/spirulina MNPs as catalysts. These results show that the spirulina and TPP do not have a catalytic role individually (Table 2, entries 2 and 3). These observations show that the reaction cycle is mainly catalyzed by spirulina and TPP as simultaneous species supports on the Fe₃O₄/KCC-1/IG nanostructure (Table 2, entry 4). As a result, Fe₃O₄/KCC-1/IG MNPs were used in the subsequent investigations because of their high reactivity, high selectivity and easy separation. Also, the activity and selectivity of the nano-catalyst can be manipulated by tailoring the chemical and physical properties in terms of size, shape, composition and morphology. To assess the exact impact of the presence of KCC-1 in the catalyst, the Fe₃O₄/KCC-1/IG MNPs were compared with Fe₃O₄/SiO₂/IG MNPs. To check this, we looked at Fe₃O₄/SiO₂/IG and Fe₃O₄/KCC-1/IG MNPs, which have the same compositions and different structures. When Fe₃O₄/SiO₂/IG was used as the catalyst, the yield of the desired product was fair to average, but the yield for Fe₃O₄/KCC-1/IG MNPs was excellent (Table 2, entries 4 and 5). Fe₃O₄/KCC-1/IG MNPs have Lewis acidic ($-\text{NH}_3^+$) and Lewis basic ($-\text{OH}^-$) sites, simultaneously. This structure results in high activity of the catalyst.

The reaction conditions were optimized by α -amino acid, ethylene oxide, and carbon dioxide application for *N*-[(2-hydroxyethoxy)carbonyl]glycine synthesis catalyzed by Fe₃O₄/KCC-1/IG MNPs in this model system. The model reaction provided examinations of the effects of different parameters like solvent (Table 3). Various solvents were applied to study their impacts on the synthesis of Fe₃O₄/KCC-1/IG MNPs (Table 3, entries 1–15). The obtained results demonstrated no formation of the expected product with polar protic solvents, including water, ethanol, methanol, and isopropanol. The cross-coupling product showed a relatively

Table 3 Synthesis of *N*-[(2-hydroxyethoxy)carbonyl]glycine by Fe₃O₄/KCC-1/IG MNPs in different solvents^a

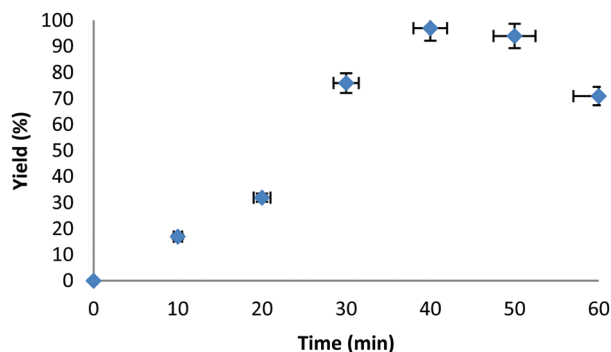
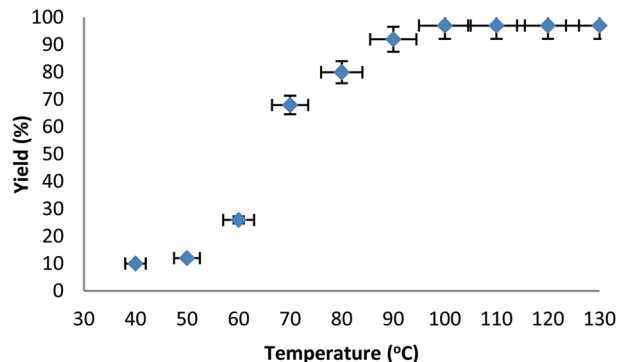
Entry	Solvent	Yield ^b (%)
1	EtOH	—
2	H ₂ O	—
3	MeOH	—
4	<i>i</i> -PrOH	—
5	THF	35
6	CH ₂ Cl ₂	34
7	EtOAc	46
8	DMF	31
9	CH ₃ CN	39
10	CHCl ₃	37
11	DMSO	43
12	Anisole	52
13	<i>n</i> -Hexane	—
14	Cyclohexane	—
15	CCl ₄	—
16	Solvent-free	97

^a Reaction conditions: appropriate α -amino acid (1.0 mmol), ethylene oxide (1.0 mmol), Fe₃O₄/KCC-1/IG MNPs (10 mg), solvent (10 mL), and CO₂ 2.0 MPa, at 100 °C. ^b Isolated yields.

average yield with DMF, EtOAc, and DMSO as polar aprotic solvents. In this research, solvents were found to have less efficiency than conventional heating under solvent-free conditions (Table 3, entry 16). When the reaction was conducted in less polar solvents, such as anisole or toluene, the average yields of the carbonylative cross-coupling product were isolated, while a low yield was obtained in polar solvents.

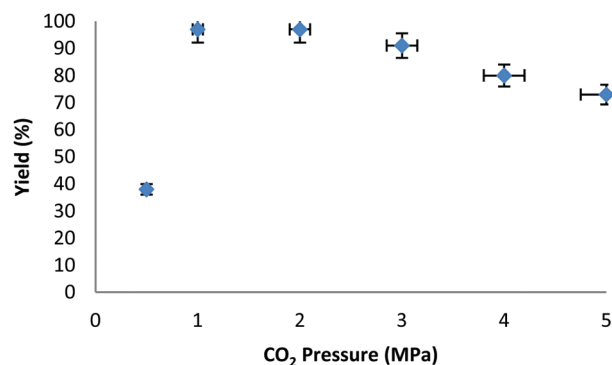
The *N*-[(2-hydroxyethoxy)carbonyl]glycine yield *versus* reaction time was depicted in Fig. 7. *N*-[(2-hydroxyethoxy)carbonyl]glycine yield increased quickly with increasing reaction time before 30 min. The increasing trend slowed down and the highest transformation was obtained at 40 min. Protracted reactions beyond 40 min resulted in the reduction of *N*-[(2-hydroxyethoxy)carbonyl]glycine yields. It looks that the formed *N*-[(2-hydroxyethoxy)carbonyl]glycine enhanced the viscosity of the reaction system to obstruct the interplay between the catalyst and reactants at longer reaction times.⁴⁹ Thus, 40 min was established as the optimum reaction time.

Fig. 8 illustrates the dependence of the *N*-[(2-hydroxyethoxy)carbonyl]glycine yield on temperature at 1 MPa, 40 min and 40–130 °C. It is revealed that the reaction temperature has a

**Fig. 7** Effect of time on the yield of *N*-[(2-hydroxyethoxy)carbonyl]glycine.**Fig. 8** Effect of temperature on the yield of *N*-[(2-hydroxyethoxy)carbonyl]glycine.

notable influence on the activity of the catalyst. The reality that high temperature is useful to the *N*-[(2-hydroxyethoxy)carbonyl]glycine production illustrates that the coupling reactions are thermodynamically desirable.^{50–52} With the increase of temperature from 40 °C to 130 °C, the *N*-[(2-hydroxyethoxy)carbonyl]glycine yields significantly rose from 10% to 97%; thus high temperature is useful to the coupling reaction. However, it is widely reported that the cycloaddition reactions of CO₂ with ethylene oxide are typically exothermic processes, so in the viewpoint of its thermodynamic equilibrium, higher temperatures may contain the cyclic carbonate formation.^{53,54} Furthermore, higher temperatures are liable to lead to the polymerization of the *N*-[(2-hydroxyethoxy)carbonyl]glycine, and therefore worsen the catalytic productivity.⁵⁵ Considering the above results and high conversion of 97%, experiments of higher temperature were not carried out and 100 °C was adopted as the optimal reaction temperature.

Also, to optimize the yield of *N*-[(2-hydroxyethoxy)carbonyl]glycine and evaluate the catalytic performances of our Fe₃O₄/KCC-1/IG MNPs, the effect of CO₂ pressure was investigated. The cycloaddition reaction between α -amino acid, ethylene oxide, and carbon dioxide catalyzed by Fe₃O₄/KCC-1/IG MNPs was examined systematically as a model reaction system (Fig. 9). Since the diffusion may affect the kinetics of reactions in the mass transfer accompanied by the reaction between α -amino acid, ethylene oxide, and carbon dioxide, an optimum CO₂ pressure range for the maximum yield of Fe₃O₄/KCC-1/IG MNPs must exist.

**Fig. 9** Effect of CO₂ pressure on the synthesis of *N*-[(2-hydroxyethoxy)carbonyl]glycine.

The pressure effect investigation was carried out in the range of 0.5–5.0 MPa. As shown in Fig. 9, the Fe₃O₄/KCC-1/IG MNP yield increased sharply when the CO₂ pressure increased from 0.5 to 1.0 MPa, and then stabilized at CO₂ pressure ranges of 1.0–2.0 MPa. Nevertheless, a reduced yield was obtained as soon as the pressure reached 3.0 MPa. Based on their reports, it could be explained that in the low-pressure region, higher CO₂ pressure could increase the CO₂ concentration in the reaction system to enhance the yield; however, too high CO₂ pressure would decrease the ethylene oxide concentration in the vicinity of the catalyst to lower the *N*-[(2-hydroxyethoxy)carbonyl]glycine yield, and a lower ethylene oxide concentration is unfavorable to the reaction because ethylene oxide is also a reactant.^{56,57} The competition between these opposite factor gave rise to an optimal pressure of 1.0 MPa for the best *N*-[(2-hydroxyethoxy)carbonyl]glycine yields.

With the optimized conditions in hand, propylene oxide could also be employed to synthesize *N*-[(2-hydroxyethoxy)carbonyl]glycine in high yields (Table 4, entry 1). Furthermore, we were interested to study the generality of the transformation with different amines. With the use of the combination of Fe₃O₄/KCC-1/IG MNPs as catalysts at 100 °C in 40 min, different amine nucleophiles could be converted to the corresponding *N*-aryl carbamates in good to excellent yields. When anilines were used, good to excellent yields were obtained. A variety of

Table 4 Synthesis of products of various amines with propylene oxide, CO₂ in the presence of the Fe₃O₄/KCC-1/IG MNPs^a

Entry	Amine	Product ratio 1 : 2	Yield ^b (%)
1		40 : 60	89
2		35 : 65	86
3		40 : 60	94
4		42 : 58	74
5		35 : 65	68
6		40 : 60	98
7		50 : 50	94
8		45 : 55	75
9		45 : 55	89
10		40 : 60	90
11		45 : 55	94

^a Reaction conditions: appropriate CO₂ (1.0 MPa), amines (1.0 mmol), propylene oxide (1.0 mmol), Fe₃O₄/KCC-1/IG MNPs (10 mg), and CO₂ 1.0 MPa, at 100 °C. ^b Isolated yield.

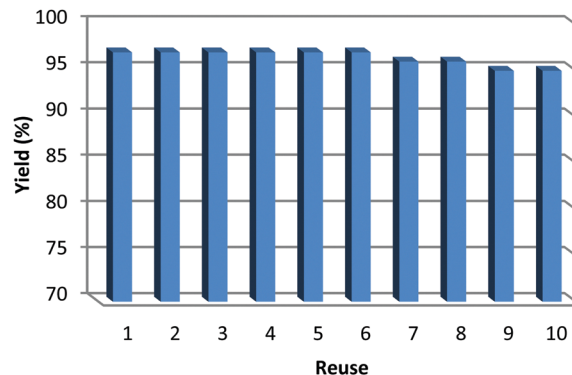


Fig. 10 The reusability of the catalysts for the synthesis of *N*-[(2-hydroxyethoxy)carbonyl]glycine.

functional groups are tolerated in this procedure, including electron-donating and, remarkably, even electron-withdrawing groups such as -F, -I, and -CN (Table 4, entries 3–5). We discovered a relatively high yield of the product to occur in the reactions with electron-donating groups. For example, -CH₃, and -OC₂H₅ produced *N*-aryl carbamate yields of 98%, and 94%, respectively (Table 4, entries 6 and 7). As shown in Table 4, various electron-donating and electron-withdrawing groups give the desired products with appreciable yields. In contrast, a dramatic effect is observed in the case of aliphatic amines. Also, an exciting effect is observed in the case of aliphatic amines under similar reaction conditions in good yields (Table 4, entries 8–11).

The reusability of the Fe₃O₄/KCC-1/IG MNP catalyst was also investigated. It was observed that it can be reused for up to ten runs without much loss in its catalytic activity, an essential aspect of green chemistry. The reusability of the Fe₃O₄/KCC-1/IG MNP catalyst upon ten consecutive runs, was also investigated in the synthesis of *N*-[(2-hydroxyethoxy)carbonyl]glycine under the optimized conditions. The catalyst could be recycled easily followed by washing several times with ethanol. It was then dried at room temperature and was recycled ten consecutive times with almost unaltered catalytic activity (Fig. 10).

Conclusions

In the present study Fe₃O₄/KCC-1/IG MNPs was synthesized and characterized as an environmentally-friendly nanocatalyst for the synthesis of *N*-[(2-hydroxyethoxy)carbonyl]glycine from carbon dioxide, ethylene oxide, and α -amino acid. The experimental results displayed the core-shell structure of the synthesized catalyst with a mean size range of 250–300 nm. In addition, the catalyst was easily recoverable and reusable. Subsequently, high yields in short reaction times were achieved without the need for an expensive catalyst as well as excellent reusability for at least ten runs in the corresponding reaction without a reduction in catalytic activity.

Conflicts of interest

There are no conflicts to declare.

Notes and references

- M. North, R. Pasquale and C. Young, *Green Chem.*, 2010, **12**, 1514–1539.
- K. Soga, Y. Tazuke, S. Hosoda and S. Ikeda, *J. Polym. Sci., Polym. Chem. Ed.*, 1977, **15**, 219–229.
- B. Ochiai and E. T. Prog, *Polym. Sci.*, 2005, **30**, 183–215.
- J. Bayardon, J. Holz, B. Schaffner, V. Andrushko, S. Verevkin, A. Preetz and A. Borner, *Angew. Chem., Int. Ed.*, 2007, **46**, 5971–5974.
- T. Tsuda, K. Kondo, T. Tomioka, Y. Takahashi, H. Matsumoto, S. Kuwabata and C. L. Hussey, *Angew. Chem., Int. Ed.*, 2011, **50**, 1310–1313.
- J. Thielen, W. H. Meyer and K. Landfester, *Chem. Mater.*, 2011, **23**, 2120–2129.
- W. Peppel, *J. Ind. Eng. Chem.*, 1958, **50**, 767–770.
- A. A. A. Shamsuzzaman and B. Khan, *Synth. Commun.*, 2010, **40**, 2278–2283.
- Z. Zhang, F. Fan, H. Xing, Q. Yang, Z. Bao and Q. Ren, *ACS Sustainable Chem. Eng.*, 2017, **5**, 2841–2846.
- A. A. G. Shaikh and S. Sivaram, *Chem. Rev.*, 1996, **96**, 951–976.
- M. North and R. Pasquale, *Angew. Chem., Int. Ed.*, 2009, **48**, 2946–2948.
- P. Yan and H. W. Jing, *Adv. Synth. Catal.*, 2009, **351**, 1325–1332.
- L. Jin, Y. Huang, H. Jing, T. Chang and P. Yan, *Tetrahedron: Asymmetry*, 2008, **19**, 1947–1953.
- R. L. Paddock and S. T. Nguyen, *Chem. Commun.*, 2004, 1622–1623.
- T. Chang, L. Jin and H. Jing, *ChemCatChem*, 2009, **1**, 379–383.
- D. J. Darensbourg and R. M. Mackiewicz, *J. Am. Chem. Soc.*, 2005, **127**, 14026–14038.
- C. Lang, Y. Shuangfeng, L. Wenhua, Z. Yuanyuan, L. Shenglian and A. Chak-tong, *Catal. Lett.*, 2010, **137**, 74–80.
- A. Baba, T. Nozaki and H. Matsuda, *Bull. Chem. Soc. Jpn.*, 1987, **60**, 1552–1554.
- Y. Tsutsumi, K. Yamakawa, M. Yoshida, T. Ema and T. Sakai, *Org. Lett.*, 2010, **12**, 5728–5731.
- P. Brignou, M. Priebe Gil, O. Casagrande, J. F. Carpentier and S. M. Guillaume, *Macromolecules*, 2010, **43**, 8007–8017.
- D. Tian, B. Liu, Q. Gan, H. Li and D. J. Darensbourg, *ACS Catal.*, 2012, **2**, 2029–2035.
- D. J. Coady, H. W. Horn, G. O. Jones, H. Sardon, A. C. Engler, R. M. Waymouth, J. E. Rice, Y. Y. Yang and J. L. Hedrick, *ACS Macro Lett.*, 2013, **2**, 306–312.
- M. Selva, A. Caretto, M. Noè and A. Perosa, *Org. Biomol. Chem.*, 2014, **12**, 4143–4155.
- P. Olsén, M. Oschmann, E. V. Johnston and B. Åkermark, *Green Chem.*, 2018, **20**, 469–475.
- A. Vonshak, A. Abeliovich, S. Boussiba, S. Arad and A. Richmond, *Biomass*, 1982, **2**, 175–185.
- G. Torzillo, P. Bernardini and J. Masojídek, *J. Phycol.*, 1998, **34**, 504–510.
- B. M. E. Chagas, C. Dorado, M. J. Serapiglia, C. A. Mullen, A. A. Boateng, M. A. F. Melo and C. H. Ataíde, *Fuel*, 2016, **179**, 124–134.
- S. M. Sadeghzadeh, R. Zhiani and S. Emrani, *Catal. Lett.*, 2018, **148**, 119–124.
- D. Akin, A. Yakar and U. Gündüz, *Water Environ. Res.*, 2015, **87**, 425–436.
- K. H. Liew, M. Rocha, C. Pereira, A. L. Pires, A. M. Pereira, M. A. Yarmo, J. C. Juan, R. M. Yusop, A. F. Peixoto and C. Freire, *ChemCatChem*, 2017, **23**, 3930–3941.
- A. Jain, K. Thakur, G. Sharma, P. Kush and U. K. Jain, *Carbohydr. Polym.*, 2016, **137**, 65–74.
- V. Polshettiwar, D. Cha, X. Zhang and J. M. Basset, *Angew. Chem.*, 2010, **49**, 9652–9656.
- A. Maity and V. Polshettiwar, *ChemSusChem*, 2017, **10**, 3866–3913.
- P. K. Kundu, M. Dhiman, A. Modak, A. Chowdhury and V. Polshettiwar, *ChemPlusChem*, 2016, **81**, 1142–1146.
- P. Gautam, M. Dhiman, V. Polshettiwar and B. M. Bhanage, *Green Chem.*, 2016, **18**, 5890–5899.
- A. Fihri, D. Cha, M. Bouhrara, N. Almana and V. Polshettiwar, *ChemSusChem*, 2012, **5**, 85–89.
- A. Fihri, M. Bouhrara, U. Patil, D. Cha, Y. Saih and V. Polshettiwar, *ACS Catal.*, 2012, **2**, 1425–1431.
- A. S. Lilly Thankamony, C. Lion, F. Pourpoint, B. Singh, A. J. Perez Linde, D. Carnevale, G. Bodenhausen, H. Vezin, O. Lafon and V. Polshettiwar, *Angew. Chem.*, 2015, **54**, 2190–2193.
- N. D. Petkovich and A. Stein, *Chem. Soc. Rev.*, 2013, **42**, 3721–3739.
- C. M. Parlett, K. Wilson and A. F. Lee, *Chem. Soc. Rev.*, 2013, **42**, 3876–3893.
- S. M. Sadeghzadeh, R. Zhiani, S. Emrani and M. Ghabdian, *RSC Adv.*, 2017, **7**, 50838–50843.
- S. M. Sadeghzadeh, R. Zhiani, M. Khoobi and S. Emrani, *Microporous Mesoporous Mater.*, 2018, **257**, 147–153.
- S. M. Sadeghzadeh, *Microporous Mesoporous Mater.*, 2016, **234**, 310–316.
- S. M. Sadeghzadeh, *J. Mol. Liq.*, 2016, **223**, 267–273.
- S. M. Sadeghzadeh, *J. Mol. Catal. A: Chem.*, 2016, **423**, 216–223.
- S. M. Sadeghzadeh, *Catal. Sci. Technol.*, 2016, **6**, 1435–1441.
- S. M. Sadeghzadeh, *Catal. Commun.*, 2015, **72**, 91–96.
- S. M. Sadeghzadeh, *Green Chem.*, 2015, **17**, 3059–3066.
- D. S. Bai, H. W. Jing and G. J. Wang, *Appl. Organomet. Chem.*, 2012, **26**, 600–603.
- R. J. Wei, X. H. Zhang, B. Y. Du, Z. Q. Fan and G. R. Qi, *RSC Adv.*, 2013, **3**, 17307–17313.
- J. L. Song, B. B. Zhang, P. Zhang, J. Ma, J. L. Liu, H. L. Fan, T. Jiang and B. X. Han, *Catal. Today*, 2012, **183**, 130–135.
- W. G. Cheng, Z. Z. Fu, J. Q. Wang, J. Sun and S. J. Zhang, *Synth. Commun.*, 2012, **42**, 2564–2573.
- J. Xu, F. Wu, Q. Jiang and Y. X. Li, *Catal. Sci. Technol.*, 2015, **5**, 447–454.
- J. Xu, F. Wu, Q. Jiang, J. K. Shang and Y. X. Li, *J. Mol. Catal. A: Chem.*, 2015, **403**, 77–83.
- L. Han, H. Li, S. J. Choi, M. S. Park, S. M. Lee, Y. J. Kim and D. W. Park, *Appl. Catal., A*, 2012, **429**, 67–72.
- Y. Xie, Z. F. Zhang, T. Jiang, J. L. He, B. X. Han, T. B. Wu and K. L. Ding, *Angew. Chem., Int. Ed.*, 2007, **46**, 7255–7258.
- L. F. Xiao, F. W. Li, J. J. Peng and C. G. Xia, *J. Mol. Catal. A: Chem.*, 2006, **253**, 265–269.